Time-Resolved Mechanistic Depiction of Photoinduced CO 2 Reduction Catalysis on a Urea-Modified Iron Porphyrin

Daniel H Cruz Neto, Eva Pugliese, Philipp Gotico, Annamaria Quaranta, Winfried Leibl, Karine Steenkeste, Daniel Peláez, Thomas Pino, Zakaria Halime, Minh-huong Ha-Thi

RESEARCH ARTICLE

Time-Resolved Mechanistic Depiction of Photoinduced CO_2 Reduction Catalysis on a Urea-Modified Iron Porphyrin

Daniel H. Cruz Neto,[a] Eva Pugliese,[b] Philipp Gotico,[c] Annamaria Quaranta,[c] Winfried Leibl,[c] Karine Steenkeste,[a] Daniel Peláez,[a] Thomas Pino,*[a] Zakaria Halime,*[b] Minh-Huong Ha-Thi*[a]

[a] D. H. Cruz Neto, Dr. K. Steenkeste, Prof. D. Peláez, Dr. T. Pino, Dr. M.-H Ha-Thi
Institut des Sciences Moléculaires d'Orsay (ISMO)
Université Paris-Saclay, CNRS
91405 Orsay – France
E-mail: thomas.pino@universite-paris-saclay.fr, minh-huong.ha-thi@universite-paris-saclay.fr

[b] Dr. E. Pugliese, Dr. Z. Halime
Institut de Chimie Moléculaire et des Matériaux d'Orsay (ICMMO)
Université Paris-Saclay, CNRS
91400 Orsay – France
E-mail: zakaria.halime@universite-paris-saclay.fr

[c] Dr. P. Gotico, Dr. A. Quaranta, Dr. W. Leibl
Institute for Integrative Biology of the Cell (I2BC)
Université Paris-Saclay, CEA, CNRS
91198 Gif-sur-Yvette – France

Abstract: The development of functional artificial photosynthetic devices relies on the understanding of mechanistic aspects involved in specialized photocatalysts. Modified iron porphyrins have long been explored as efficient catalysts for the light-induced reduction of carbon dioxide (CO_2) towards solar fuels. In spite of the advancements in homogeneous catalysis, the development of the next generation of catalysts requires a complete understanding of the fundamental photoinduced processes taking place prior to and after activation of the substrate by the catalyst. In this work, we employ a state-of-the-art nanosecond optical transient absorption spectroscopic setup with a double excitation capability to induce charge accumulation and trigger the reduction of CO_2 to carbon monoxide (CO). Our biomimetic system is composed of a urea-modified iron(III) tetraphenylporphyrin ($UrFe^{III}$) catalyst, the prototypical $[Ru(bpy)_3]^{2+}$ (bpy = 2,2'-bipyridine) used as a photosensitizer, and sodium ascorbate as an electron donor. Under inert atmosphere, we show that two electrons can be successively accumulated on the catalyst as the fates of the photogenerated $UrFe^{II}$ and $UrFe^{I}$ reduced species are tracked. In the presence of CO_2, the catalytic cycle is kick-started providing further evidence on CO_2 activation by the UrFe catalyst in its formal Fe^{I} oxidation state.

Introduction

High-energy demands coupled with a widespread exploitation of fossil fuels, leading to the emission of huge quantities of greenhouse gases in the atmosphere, are problems that call out for urgent solutions. Amongst the sustainable and renewable sources of energy available to human utilization, sunlight is the most promising option.[1–4] Nature is usually taken as an inspiration source for scientific and technological developments in attempts to harness this invaluable energy input.[5]

Natural photosynthesis is the evolutionary masterpiece that allowed life to evolve on earth and is often seen as a guiding light to the development of novel solar-to-fuel devices.[2–4,6,7] The processes taking place in molecular photosystems within photosynthetic organisms set the stage and the rules of the biomimicry game. These rules inform scientists on the functional requirements for an artificial system – light absorption followed by charge separation and accumulation of redox equivalents on highly efficient catalysts capable of multielectronic bond-breaking and bond-formation reactivity.[8–10]

Molecular catalysis has paved the way to the development of highly active, selective, and efficient homogeneous catalysts for the thermodynamically and kinetically demanding CO_2 reduction reaction. Amongst a myriad of catalysts, iron tetraphenylporphyrin (FeTPP) derivatives have been shown to be promising candidates, mainly due to the possibility of introducing second coordination sphere functionalities that can interact with the substrate and provide a microenvironment that facilitates the subsequent activation and transformation of CO_2.[11–20]

Although these catalysts have shown improved catalytic performances under optimized conditions, with record-breaking turnover numbers and frequencies,[11–18,21,22] their further optimization towards real application levels requires a proper understanding of the fundamental light-induced processes they host when coupled to a photosensitizer. This is often seen as a bottleneck on the development of the next generation of photocatalysts since information on structure-activity relationships are essential to guide their design and optimization.

It is in this context that time-resolved spectroscopic techniques come into play. The development of pump-probe and pump-pump-probe experimental strategies has provided the lens through which one can scrutinize the very fundamental photophysical and photochemical events in the functioning and

dynamics of active biomimetic photosystems. Even though important studies on reversible charge accumulation in multicomponent photosystems have been recently reported,[23–25] they mostly cover catalytically inactive systems, focusing on electron transfer and recombination processes under inert atmosphere.

Taking a step forward against this background, this study aims at investigating the reversible light-induced charge accumulation dynamics on an active catalytic system under inert atmosphere and its behavior when subjected to catalytic conditions in the presence of CO_2 as a substrate and H_2O as a proton source. To probe the photodynamics of such a system, we employ a state-of-the-art nanosecond optical transient absorption (OTA) spectroscopic technique, with both single and double excitation capabilities. In addition, a resonance Raman probe was used to further characterize the photogenerated species via their vibrational features.

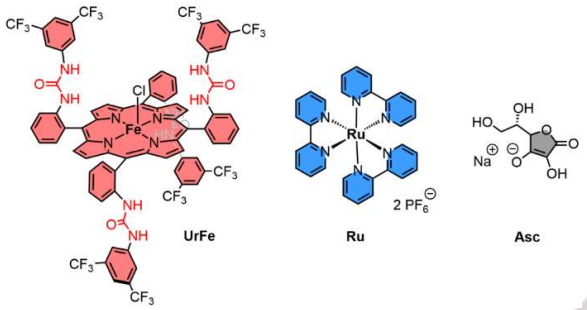

Figure 1. Active multicomponent system with UrFe as a CO_2 reduction catalyst, $[Ru(bpy)_3]^{2+}$ (Ru) as a photosensitizer, and sodium ascorbate (Asc) as an electron donor.

Herein, the CO_2 reduction catalyst is an iron tetraphenylporphyrin derivative bearing four urea arms (UrFe) whose design is inspired by the active site of the carbon monoxide dehydrogenase (CODH) enzyme (Figure 1). The urea groups in the second coordination sphere are positioned in an *αβαβ* geometry and engage in a multipoint hydrogen-bonding interaction with iron-bonded CO_2 adducts, resulting in an outstanding catalytic performance for the CO_2-to-CO reduction.[26,27] Recent studies[28,29] have shown that UrFe interacts with CO_2 at its formal Fe^{I} state. This has prompted us to look deeper into the formation kinetics of this state using time-resolved spectroscopy. This approach allows us to better comprehend the kinetics of charge transfer and accumulation leading to catalytic activation of CO_2, which lies far beyond what is covered by steady-state spectroscopy in previous reports.[28,29] The complete photosystem (Figure 1) is constituted of the prototypical $[Ru(bpy)_3]^{2+}$ (Ru) photosensitizer, sodium ascorbate (Asc) as an electron donor and UrFe as the catalyst in an acetonitrile/water (CH_3CN/H_2O 6:4) solvent mixture. It is noteworthy that the commonly used sacrificial electron donor 1,3-dimethyl-2-phenyl-2,3-dihydro-1*H*benzo[*d*]imidazole (BIH), was substituted in this study by ascorbate as a reversible electron donor in order to explore the dynamics of both electron transfer and charge recombination processes.

Results and Discussion

In the presence of sodium ascorbate (Figure S2), a red shift is observed in the Soret band of $UrFe^{III}$ centered at 417 nm (ε ~ 1.1×10^5 $M^{-1}cm^{-1}$ in a CH_3CN/H_2O 6:4 mixture), which can be attributed to a minor formation of $UrFe^{II}$ in the dark. This dark reaction is further confirmed by electron paramagnetic resonance (EPR) measurements (Figure S3), which shows a decrease in the signal of $UrFe^{III}$ due to the formation of EPR-silent Fe^{II} in the presence of Asc. The addition of the Ru photosensitizer in this mixture results in a weighted sum of the specific spectral contributions of each component (Figure S4), indicating negligible interaction amongst them in the ground state. In all time-resolved experiments herein presented, the photosensitizer is excited at its ^{3}MLCT absorption band at 460 nm with a fixed laser energy of ~1.8 mJ/pulse and a spot size of ~9 mm^2.

For time-resolved experiments, samples containing UrFe (7.6 μM), Ru (35 μM), and Asc (100 mM) in CH_3CN/H_2O (6:4) were used and vigorous stirring was maintained during the measurements. Excitation of the photosensitizer alone (Figure S5) led to its ground state bleaching and formation of ~14.2 (±1.4) μM (ΔA_{450} = -0.16, using $\Delta\varepsilon_{450}$ = -11300 $M^{-1}cm^{-1}$)[30] of its triplet excited state, ^{3}Ru*, corresponding to ~41% of the ground state population. When Asc is added to the solution, reductive quenching of ^{3}Ru* takes place, reversibly creating ~10.8 (±1.1) μM (ΔA_{500} = 0.13, using $\Delta\varepsilon_{500}$ = 12000 $M^{-1}cm^{-1}$)[31] of its reduced state (denoted Ru^+) which can later recombine with oxidized ascorbate (denoted Asc^+) to regenerate the ground state (Figure S6). Formation and recombination rate constants were estimated to be 2.8 (±0.9) $\times10^8$ $M^{-1}s^{-1}$ and 3.0 (±0.9) $\times10^9$ $M^{-1}s^{-1}$, respectively.[9,25] The efficiency of charge separation was ~76% of the ^{3}Ru* population.

In a multicomponent solution containing also UrFe, based on its redox potentials (vs. NHE) previously reported in the literature (Table S1),[27] the thermodynamic landscape of Ru^+ would bear two possible favorable reductions of the porphyrin, generating Fe^{II} (ΔG_{ET} = -1.31 V) and the formal Fe^{I} (ΔG_{ET} = -0.43 V) oxidation states.[27] Therefore, under such conditions, up to two electrons may be accumulated on the catalyst. Of note, we choose to maintain the commonly used formulation of both formal Fe^{I} and Fe^{0} species in the text for simplicity. However, we advert to recent studies[32–37] where the second and third reductions of iron porphyrins have generally been regarded as ligand-centered, and so a more appropriate formulation of the aforementioned species would be [$Fe^{II}porph^{\bullet-}$] and [$Fe^{II}porph^{\bullet2-}$] (with porph = porphyrin), respectively.

In the presence of UrFe, snapshots of transient absorption measurements with a single excitation pump can be divided into three time windows (Figure 2, left panel). Up to 140 ns (Figure 2a), reductive quenching of the photosensitizer's excited state is observed, with the positive absorption band of Ru^+ rising at 500 nm. Along with the decay of the reactive Ru^+ species, the first electron transfer from Ru^+ to Fe^{III} takes place, generating Fe^{II} with an absorption band centered at 436 nm (Figure 2b). The nature of this reduced species is also confirmed using UV-Vis spectroelectrochemistry experiments (SEC, Figures S7 and S8). Simulations of the kinetics involving the abovementioned

photogenerated species (Figure 2, right panel) performed with a previously reported numerical method[38] allowed us to extract an electron transfer rate constant of k_{et1} = 9.6 (±2.9) ×10^9 M^{-1}s^{-1} for this process which is close to the diffusion limit.

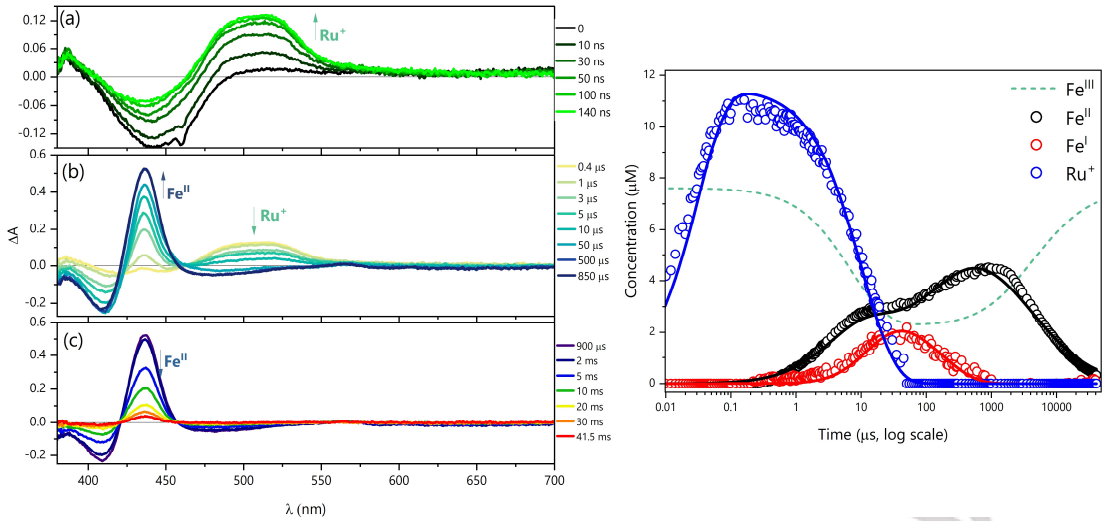

Figure 2. Single pump OTA spectra of a mixture composed of UrFe (7.6 µM), Ru (35 µM), and Asc (100 mM) in CH_3CN/H_2O (6:4) divided into windows of (a) 0 to 140 ns, (b) 0.4 to 850 µs, and (c) 0.9 to 41.5 ms (left panel). Concentration profile of photogenerated species obtained from kinetic simulations (right panel). λ_{exc} = 460 nm, 1.8 mJ/pulse.

However, by tracing the kinetics related to Fe^{II} (Figure 2, right panel), one may realize that an extra process is taking place, evidenced by a second rise in the concentration of Fe^{II} between 100 µs and 800 µs. This suggests a reversible single-pump-induced charge accumulation generating the doubly-reduced Fe^{I} species. The formation of this species is the result of two sequential electron transfer processes that are likely to occur when the concentration of the photoreductant (here Ru$^+$) is comparable or higher than that of the species to be reduced (Fe^{II}).[9,25,38] Indeed, a plot of [Fe^{I}]/[Fe^{II}] as a function of the laser energy shows a proportionality relationship (Figure S9), which is expected for this 2-electron process. Kinetic simulations indicate the formation of ~2.1 (±0.2) µM of Fe^{I} in solution (red trace in Figure 2, right panel) with k_{et2} = 9.3 (±2.8) ×10^9 M^{-1}s^{-1}, which is close to the diffusion limit as observed for k_{et1}. In turn, the decay of Fe^{I} was simulated with two different relaxation pathways: (i) reaction of Fe^{I} with oxidized ascorbate with k_{rec2} = 1.5 (±0.4) ×10^8 M^{-1}s^{-1} and (ii) a comproportionation reaction between Fe^{I} and Fe^{III} (ΔG_{ET} = -0.47 V) with k_{recb} = 3.8 (±1.2) ×10^8 M^{-1}s^{-1}. These relaxation processes lead to the second rising phase of Fe^{II} in the right panel of Figure 2, generating its maximal concentration of 4.5 (±0.5) µM approximately 800 µs after the excitation. Details on the simulations are available in the SI.

Finally, for longer delay times (Figure 2c), the recombination of Fe^{II} with Asc$^+$ is observed with k_{rec1} = 4.2 (±1.3) ×10^7 M^{-1}s^{-1}, and the system recovers its ground state with no noticeable change in its absorption features, excluding any degradation under the operational experimental conditions (Figure S10). However, this recombination reaction is notably slow, leading to the accumulation of Fe^{II} and Asc$^+$ in solution in the timeframe of the experiment (maximal instrumental pump-probe delay of ~41.5 ms) even under vigorous stirring.

To induce an efficient accumulation of charge, a second laser pump operating at the same excitation wavelength and the same energy was fired 800 µs after the first one. This delay time corresponds to approximately the maximal concentration of Fe^{II} generated by the first pump where also Ru$^+$ has completely returned to its ground state so that it is ready to perform a second photoredox reaction to produce more of the formal Fe^{I} charge-accumulated state.

Indeed, double pump transient absorption spectra recorded in the online subtraction mode[24] show a much clearer formation of an Fe^{I} species (Figure 3a) from the reaction between Fe^{II} and the Ru$^+$ generated by the second excitation. The maximal concentration of the charge-accumulated species was observed at a delay of ~30 µs. The spectral signature of formal Fe^{I} is observed at 460 nm (comparison with a reference spectrum in Figure S11). On a longer timescale, recombination with Asc$^+$ takes place, giving rise to Fe^{II} as the band corresponding to Fe^{I} decays (Figure 3b). The subsequent decay of Fe^{II} is in turn due to an analogous recombination reaction with Asc$^+$ (Figure 3c) in such a reversible system. With respect to the single pump, the maximal transient concentration of formal Fe^{I} is two times higher when the double excitation strategy is used (Figure S12), making its formation more evident and allowing us to obtain a clear spectroscopic signature that confirms its identity beyond doubt. The same kinetic model was used to simulate the double pump OTA experiments recorded in normal mode (Figure S13) and the time-dependent evolution of relevant species is shown on the right panel of Figure 3.

A further photoinduced reduction step to the formal Fe^0 species is not observed in our experiments. This fact may be rationalized by an uphill redox process when Ru$^+$ is used as the reducing species (ΔG_{ET} = 40 mV), making this electron transfer

reaction thermodynamically unfavorable. We note that, for UrFe, this third reduction step is not required since the formal Fe^{I} species is already catalytically active.[28,29] In addition, starting from Fe^{III}, the photoaccumulation of three electrons to generate the formal Fe^{0} state in a reversible photosystem would be particularly challenging due to the competing and thermodynamically much more favorable charge recombination processes involving both the first and second charge-accumulated states. In line with that, our results show a clear accumulation of two charges on an active catalyst under inert atmosphere and in a reversible manner. This stepwise accumulation of two electrons has prompted us to investigate further how this species would behave under catalytic conditions.

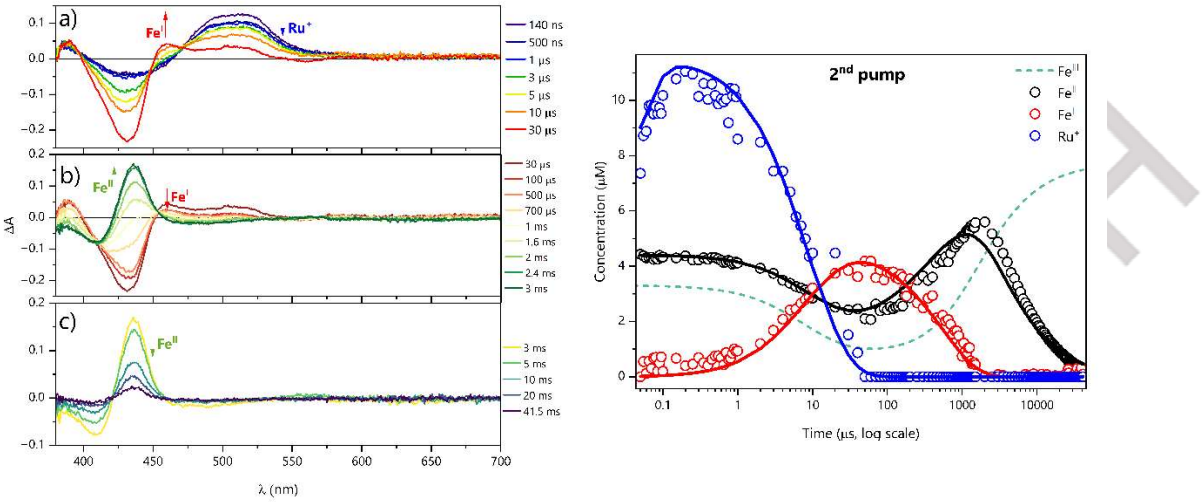

Figure 3. Double pump transient absorption spectra (in subtraction mode) of a mixture composed of UrFe (7.6 µM), Ru (35 µM), and Asc (100 mM) in CH_3CN/H_2O (6:4). The spectra were divided into time panels of (a) 140 ns to 30 µs, (b) 30 µs to 3 ms, and (c) 3 to 41.5 ms (left panel). Concentration profile of photogenerated species obtained from kinetic simulations of double pump measurements in normal mode (right panel). λ_{pump1} = 460 nm – 1.8 mJ/pulse, 20 Hz; λ_{pump2} = 460 nm – 1.8 mJ/pulse, 10 Hz; pumps delayed by 800 µs.

In the presence of CO_2, the ground state absorption spectrum of the sample is modified after a single pump laser-induced excitation (Figure 4, left panel), with the accumulation of a species characterized by an intense Soret band at 420 nm. Remarkably, this newly-formed species resembles a well-known intermediate in the photocatalytic cycle of the CO_2-to-CO reduction reaction: Fe^{II}-CO.[28,29] This species was also identified by overlaying the absorption spectrum of a chemically prepared Fe^{II}-CO solution and the spectra of the multicomponent system before and after the laser excitation (Figure 4, left).

The single pump transient absorption measurement of the sample under CO_2 atmosphere reveals yet another photophysical feature of Fe^{II}-CO: its photolability, *i.e.*, its ability to release the CO upon excitation of any electronic transition of the porphyrin.[39–44] The release of CO, once the excited state of the Fe^{II}-CO species is generated, yields the characteristic transient absorption feature shown in Figure S14.[28] In the first time window of the recorded spectra in the presence of CO_2 (Figure 4a, right panel), besides the reductive quenching mechanism creating Ru^{+}, a positive absorption band of Fe^{II} (at 436 nm) generated from the de-coordination of the axially-bound CO appears immediately with the laser excitation at 460 nm (at 0 µs). It is important to mention that a complete set of measurements involves irradiating the sample with multiple laser flashes, which results in the accumulation of Fe^{II}-CO and hence the observation of its spectral characteristics very early in the timeframe of the pump-probe experiment.

Up to 70 µs (Figure 4b), formation of Fe^{I} is observed as a result of two concomitant mechanistic pathways involving the reaction of Ru^{+} with (i) the Fe^{II} that is generated from the photolysis of $Fe^{II}CO$ and, importantly, (ii) $Fe^{II}CO$ (ΔG_{ET} = -0.26 V, Table S1). The latter process appears in the kinetics as additional loss of $Fe^{II}CO$ with an apparent kinetics of about 10 µs (Figure S17, left panel). Further steps involve a recombination of Fe^{I} with Asc^{+} (Figure 4c) and the re-coordination of CO to the Fe^{II} center of the porphyrin (Figure 4d). Double excitation measurements in this sample did not reveal any additional reduction steps.

To confirm the accumulation of Fe^{II}-CO in the sample during the pump-probe experiment, three different strategies were adopted. First, we probed the photolability of the Fe^{II}-CO species upon exciting one of the weakly absorbing Q-bands. Figure S18 presents the transient spectrum obtained 100 ns after a 605 nm laser excitation, confirming the de-coordination of CO from the Fe^{II}-CO species. Of note, since the Ru photosensitizer is not excited at 605 nm, the spectral signature of Ru^{+}, at 500 nm, is not observed in the spectrum.

Secondly, we have performed single pump OTA measurements in a second sample prepared at the same initial concentrations of all the components, but purged with CO rather than CO_2. The steady-state absorption spectrum of this mixture shows immediate formation of Fe^{II}-CO under CO atmosphere in the dark (Figure S19), demonstrating the high affinity of CO for the Fe^{II} porphyrin that is created, in this case, in a dark reaction between Fe^{III} and Asc. This is due to a significant stabilization of

the Fe^{II} redox state because of its strong binding with CO. Once again, the very same CO de-coordination step is immediately observed with the 460 nm excitation preceding the formation of Ru^{+} (Figure S16), reproducing the spectral features obtained with the CO_2-saturated sample.

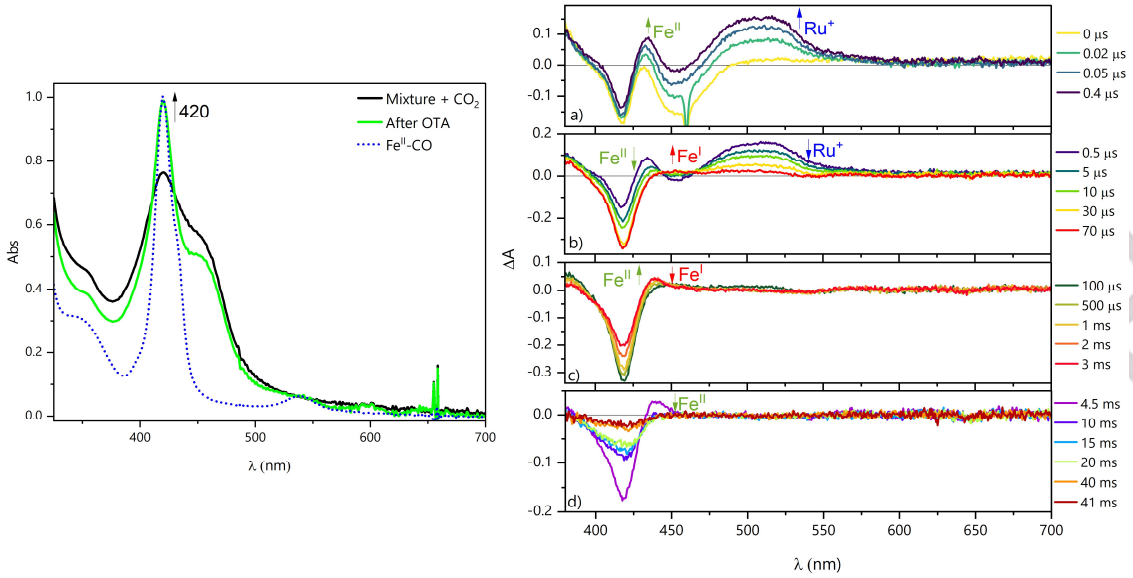

Figure 4. Absorption spectra (left panel) of the mixture containing UrFe (7.6 µM), Ru (35 µM), and Asc (100 mM) in CH_3CN/H_2O (6:4) after CO_2 bubbling (black) and after a single pump OTA measurement (green). The scaled reference spectrum of chemically produced Fe^{II}-CO is overlapped for comparison (dotted blue line). Single pump OTA of the CO_2-saturated sample (right panel) divided into time panels of (a) 0 µs to 0.4 µs, (b) 0.5 µs to 70 µs, (c) 100 µs to 3 ms, and (d) 4.5 ms to 41 ms; λ_{exc} = 460 nm, 1.8 mJ/pulse.

The complete dynamics under CO atmosphere is consistent with the same electron transfer reactions from Ru^{+} to both $Fe^{II}CO$ and photogenerated Fe^{II} up to 50 µs, yielding a very similar kinetic evolution as observed in the case of CO_2 (Figure S16, right). Finally, the decay of Fe^{I} results from its direct recombination with oxidized ascorbate (Figure S16c). These conclusions are further supported by the multiexponential analysis of the kinetics recorded under Ar, CO_2, and CO, made available in the SI (Figures S14, S20-21, and Table S2).

Finally, the specific Fe^{II}-C stretching mode in Fe^{II}-CO ($\nu_{Fe\text{-}C}$ = 524 cm^{-1})[45] was used as a spectral probe to attest the presence of Fe^{II}-CO in solution. To observe this specific Raman mode, we prepared a solution containing a higher concentration of UrFe (~11 µM) in the multicomponent mixture under CO_2 atmosphere and accumulated the intermediate species through continuous irradiation with a 456 nm LED light source (Figure S22). The higher concentration allows us to obtain a better signal-to-noise ratio in the resonance Raman spectrum. In Figure S23, the absorption spectra obtained after excitation both with pulsed and continuous irradiation sources are overlapped showing a good match. Indeed, the specific fingerprint vibrational mode of Fe^{II}-CO was detected at 524 cm^{-1} for both samples with pulsed and continuous irradiation (Figure S24), providing further proof of the sample's composition after light irradiation in the presence of the carbon dioxide substrate.

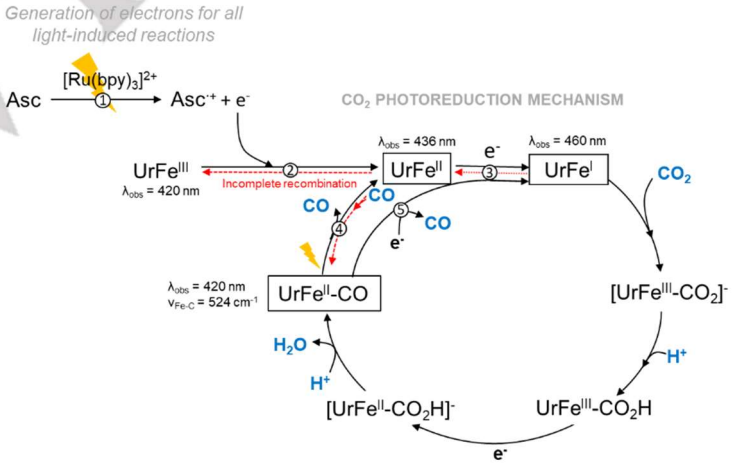

Scheme 1. Summary of all photoinduced processes of charge accumulation and CO_2 reduction taking place in a biomimetic system featuring UrFe as a catalyst. Species represented in a box are detected in our experiments, while other intermediate in the cycle were reported in the literature.[29]

In a sample initially saturated with CO_2, the accumulation of the Fe^{II}-CO species in solution observed after irradiation can only be attributed to the activation of CO_2 followed by double protonation and cleavage of the C–OH bond to release a water molecule. In our experiments, the generation of a formal Fe^0 species would be a process implying a thermodynamically uphill electron transfer reaction from Ru^+. No spectral feature or kinetic indicator for the formation of formal Fe^0 were detected in the OTA measurements using double excitation. Instead, all photoinduced processes led to a clear formation of the Fe^I species even when submitted to a single pump excitation.

These considerations are consistent with CO_2 activation and reduction by the UrFe porphyrin in its formal Fe^I state. By employing X-Ray Absorption Near Edge Spectroscopy (XANES), a recent study has provided clues that an interaction between the doubly-reduced Fe^ITPP and CO_2 is possible.[46] In another study, the formation of a formal [Fe^I-CO_2] adduct has been suggested to be the rate-determining step in the photocatalytic CO_2-to-CO conversion when UrFe is used as a catalyst BIH used as a stronger and irreversible electron donor.[28] Indeed, the urea functionalization of the second coordination sphere may provide the proper environment for binding and activation of the substrate at the metal center on the formal Fe^I species, challenging the classical picture of porphyrin-based photocatalytic CO_2 reduction.

A global picture of all light-induced processes unveiled in this work is presented in Scheme 1. In step 1, the reaction used as a source of electrons for all photoinduced events is represented. Under inert atmosphere, we show that up to two electrons can be effectively photoaccumulated on the UrFe porphyrin (steps 2 and 3), leading to the reversible formation of the formal Fe^I oxidation state. Importantly, as previously stated, the recombination of Fe^{II} with the oxidized electron donor is slow, causing their accumulation.

Remarkably, in the presence of CO_2, the steady-state absorption spectrum of the sample after a single pump irradiation showed the accumulation of Fe^{II}-CO, whose presence was further confirmed with different experimental methods. The formation of Fe^{II}-CO provides an indirect evidence of the activation of CO_2 by UrFe at its formal Fe^I oxidation state, triggering a catalytic cycle that has recently been fully explored.[28,29] Of note, oxidized ascorbate will also accumulate under catalytic condition, and so realization of a real-world application will require coupling this half-reaction to another oxidation half-reaction that can provide electrons and protons in a sustainable way.

An extensive spectroscopic investigation on the same urea-modified porphyrin has recently disclosed the full electrocatalytic cycle of CO_2 reduction by UrFe.[29] All proposed mechanistic steps are shown in Scheme 1. Once formed, Fe^I is observed to bind CO_2, generating a ferric low spin [Fe^{III}-CO_2]$^-$ species that undergoes protonation to yield a high spin Fe^{III}-CO_2H intermediate. The latter can be easily reduced to a high spin ferrous species, [Fe^{II}-CO_2H]$^-$, which in turn can be protonated leading to the C-O bond cleavage, releasing a water molecule and generating Fe^{II}-CO, the further reduction of which, as observed in this work, leads to CO release and formation of Fe^I closing the catalytic cycle (step 5 in Scheme 1). We furthermore showed that direct excitation of Fe^{II}CO will cause its partial photolysis, generating Fe^{II} (step 4) that can be reduced to Fe^I as an alternative way to close the cycle. It is noteworthy that step 5 is dominant for Fe^I generation, which is consistent with the weaker absorption of Fe^{II}-CO at 460 nm compared to that of the Ru photosensitizer, leading to only a small amount of Fe^{II} resulting from photolysis and a large remaining Fe^{II}-CO concentration after flash. A study of the dependence of pathways 4 and 5 on the initial concentration of Ru confirms this hypothesis (Figure S25).

In our system, generation of Fe^{II}-CO is observed directly with a single pump excitation. This can be partially explained by the fact that, in the initial solution, a mixture of both Fe^{III} and Fe^{II} is present once ascorbate is added. Additionally, as previously shown, Fe^{II} exhibits a slow charge recombination with Asc^+ and accumulates in solution during flash experiments. Most importantly, it is the accumulation of Ru^+ equivalents and hence the multiple unavoidable encounters with the catalyst that allows for direct production of Fe^{II}-CO. Indeed, from Fe^{II}, reduction to the formal Fe^I is afforded by Ru^+ (step 3 of Scheme 1), as well as the reduction of Fe^{III}-CO_2H, which is much easier to achieve (-1.05 V vs. Fc^+/Fc) as compared to the reduction of Fe^{II} (-1.40 V vs. Fc^+/Fc).[29]

Our measurements could only detect the reaction's most stable intermediate, Fe^{II}-CO, and none of the preceding transient intermediates. This can be explained by the fact that, at room temperature, the reactions are relatively fast, and because of the immediate availability of protons afforded by the large amount of water used in our solvent mixture, the Fe^{III}-CO_2H intermediate species undergoes fast electron and proton transfers leading to C-O bond cleavage and the observed Fe^{II}-CO. In fact, the intermediates described in the aforementioned study were trapped at -75 °C while detections were not possible at room temperature in UV-Vis experiments.[29] Nevertheless, the smaller amount of Fe^I observed in the presence of CO_2 compared to CO (Figure S17) could be an indication for its reaction with CO_2 leading to a species with a lower absorption at the observed wavelength.

Conclusion

By decoupling the processes of charge accumulation and catalysis, our results provide insights into important mechanistic steps in the photocatalytic reduction of CO_2 by a urea-modified iron porphyrin. To the best of our knowledge, this work stands as a first report of reversible multiple electron accumulation on an active multicomponent catalytic system. The photo-activation and reduction of CO_2 was evidenced to be triggered by an Fe^I active species leading to the efficient formation of Fe^{II}-CO as a $2e^-$ and $2H^+$ CO_2 reduction product. This result provides more evidence on the involvement of the formal Fe^I urea-based porphyrin as the active species in the catalytic CO_2 reduction. Further investigations are in progress to detect and explore other intermediates in the photocatalytic cycle. Such fundamental studies open a completely new avenue of mechanism exploration for iron porphyrins when used as catalysts for the CO_2-to-CO reduction in photocatalytic conditions.

Supporting Information

The authors have cited additional references within the Supporting Information.[47,48]

Acknowledgements

This work has been supported by the French National Research Agency (LOCO, grant No. ANR-19-CE05-0020-01). DHCN is grateful for the MESRI grant (2021-2024). We thank Paris-Saclay University and CNRS for additional financial support.

Keywords: Artificial Photosynthesis • Transient Absorption Spectroscopy • Charge Accumulation • Iron Porphyrin • Carbon Dioxide

[1] E. Romero, V. I. Novoderezhkin, R. Van Grondelle, *Nature* **2017**, *543*, 355–365.

[2] D. Gust, T. A. Moore, A. L. Moore, *Acc. Chem. Res.* **2009**, *42*, 1890–1898.

[3] B. Zhang, L. Sun, *Chem. Soc. Rev.* **2019**, *48*, 2216–2264.

[4] J. Barber, *Chem. Soc. Rev.* **2009**, *38*, 185–196.

[5] C. Herrero, A. Quaranta, W. Leibl, A. W. Rutherford, A. Aukauloo, *Energy Environ. Sci.* **2011**, *4*, 2353–2365.

[6] V. Balzani, A. Credi, M. Venturi, *ChemSusChem*. **2008***, 1,* 26-58..

[7] M. D. Kärkäs, O. Verho, E. V. Johnston, B. Åkermark, *Chem. Rev.* **2014**, *114*, 11863–12001.

[8] L. Hammarström, *Acc. Chem. Res.* **2015**, *48*, 840–850.

[9] T. T. Tran, M. H. Ha-Thi, T. Pino, A. Quaranta, C. Lefumeux, W. Leibl, A. Aukauloo, *J. Phys. Chem. Lett.* **2018**, *9*, 1086–1091.

[10] P. Gotico, T. T. Tran, A. Baron, B. Vauzeilles, C. Lefumeux, M. H. Ha-Thi, T. Pino, Z. Halime, A. Quaranta, W. Leibl, A. Aukauloo, *ChemPhotoChem* **2021**, *5*, 654–664.

[11] K. E. Dalle, J. Warnan, J. J. Leung, B. Reuillard, I. S. Karmel, E. Reisner, *Chem. Rev.* **2019**, *119*, 2752–2875.

[12] P. Gotico, Z. Halime, A. Aukauloo, *Dalt. Trans.* **2020**, *49*, 2381–2396.

[13] C. F. Leung, P. Y. Ho, *Catalysts* **2019**, *9*, 1-26.

[14] M. Hammouche, D. Lexa, J. M. Savêant, M. Momenteau, *J. Am. Chem. Soc.* **1991**, *113*, 8455–8466.

[15] H. Takeda, C. Cometto, O. Ishitani, M. Robert, *ACS Catal.* **2017**, *7*, 70–88.

[16] K. Takahashi, K. Hiratsuka, H. Sasaki, S. Toshima, *Chem. Lett.* **1979**, *8*, 305–308.

[17] E. Boutin, L. Merakeb, B. Ma, B. Boudy, M. Wang, J. Bonin, E. Anxolabéhère-Mallart, M. Robert, *Chem. Soc. Rev.* **2020**, *49*, 5772-5809.

[18] E. Boutin, M. Robert, *Trends Chem.* **2021**, *3*, 359–372.

[19] P. Gotico, Z. Halime, W. Leibl, A. Aukauloo, *Chempluschem* **2023**, *88*, e202300222.

[20] P. Gotico, W. Leibl, Z. Halime, A. Aukauloo, *ChemElectroChem* **2021**, *8*, 3472–3481.

[21] I. Azcarate, C. Costentin, M. Robert, J. M. Savéant, *J. Am. Chem. Soc.* **2016**, *138*, 16639–16644.

[22] D. Liu, H. Wang, T. Ouyang, J. Wang, L. Jiang, D. Zhong, T. Lu, *ACS Appl. Energy Mater.* **2018**, *1*, 2452-2459.

[23] T. H. Bürgin, O. S. Wenger, *Energy and Fuels* **2021**, 35, 1888-18856.

[24] S. Mendes Marinho, M. H. Ha-Thi, V. T. Pham, A. Quaranta, T. Pino, C. Lefumeux, T. Chamaillé, W. Leibl, A. Aukauloo, *Angew. Chemie - Int. Ed.* **2017**, *56*, 15936–15940.

[25] D. H. Cruz Neto, J. Soto, N. Maity, C. Lefumeux, T. Nguyen, P. Pernot, K. Steenkeste, D. Peláez, M. H. Ha-Thi, T. Pino, *J. Phys. Chem. Lett.* **2023**, *14*, 4789–4795.

[26] P. Gotico, B. Boitrel, R. Guillot, M. Sircoglou, A. Quaranta, Z. Halime, W. Leibl, A. Aukauloo, *Angew. Chemie - Int. Ed.* **2019**, *58*, 4504–4509.

[27] P. Gotico, L. Roupnel, R. Guillot, M. Sircoglou, W. Leibl, Z. Halime, A. Aukauloo, *Angew. Chemie - Int. Ed.* **2020**, *59*, 22451–22455.

[28] E. Pugliese, P. Gotico, I. Wehrung, B. Boitrel, A. Quaranta, M. H. Ha-Thi, T. Pino, M. Sircoglou, W. Leibl, Z. Halime, A. Aukauloo, *Angew. Chemie - Int. Ed.* **2022**, *61*, e202117530.

[29] S. Amanullah, P. Gotico, M. Sircoglou, W. Leibl, M. J. Llansola-portoles, T. Tibiletti, A. Quaranta, Z. Halime, A. Aukauloo, *Angew. Chemie - Int. Ed.* **2024**, *63*, e202314439.

[30] P. Müller, K. Brettel, *Photochem. Photobiol. Sci.* **2012**, *11*, 632–636.

[31] R. S. Khnayzer, V. S. Thoi, M. Nippe, A. E. King, J. W. Jurss, K. A. El Roz, J. R. Long, C. J. Chang, F. N. Castellano, *Energy Environ. Sci.* **2014**, *7*, 1477–1488.

[32] J. Chen, M. Li, R. Liao, *Inorg. Chem.* **2023**, *62*, 9400-9417.

[33] Y. Q. Zhang, J. Y. Chen, P. E. M. Siegbahn, R. Z. Liao, *ACS Catal.* **2020**, *10*, 6332–6345.

[34] C. Römelt, S. Ye, E. Bill, T. Weyhermüller, M. Van Gastel, F. Neese, *Inorg. Chem.* **2018**, *57*, 2141–2148.

[35] A. J. Göttle, M. T. M. Koper, *J. Am. Chem. Soc.* **2018**, *140*, 4826–4834.

[36] C. Römelt, J. Song, M. Tarrago, J. A. Rees, M. Van Gastel, T. Weyhermüller, S. Debeer, E. Bill, F. Neese, S. Ye, *Inorg. Chem.* **2017**, *56*, 4745–4750.

[37] P. A. Davethu, S. P. De Visser, *J. Phys. Chem. A* **2019**, 123, 30, 6527–6535.

[38] T. T. Tran, T. Pino, M. H. Ha-Thi, *J. Phys. Chem. C* **2019**, *123*, 28651–28658.

[39] B. I. Greene, R. M. Hochstrasser, R. B. Weisman, W. A. Eaton, *Proc. Natl. Acad. Sci. U. S. A.* **1978**, *75*, 5255–5259.

[40] B. D. Dunietz, A. Dreuw, M. Head-Gordon, *J. Phys. Chem. B* **2003**, *107*, 5623–5629.

[41] Y. Mizutani, T. Kitagawa, *J. Phys. Chem. B* **2001**, *105*, 10992–10999.

[42] S. Franzen, L. Kiger, C. Poyart, J. L. Martin, *Biophys. J.* **2001**, *80*, 2372–2385.

[43] K. Falahati, H. Tamura, I. Burghardt, M. Huix-Rotllant, *Nat. Commun.* **2018**, *9*, 1-8.

[44] A. Dreuw, B. D. Dunietz, M. Head-Gordon, *J. Am. Chem. Soc.* **2002**, *124*, 12070–12071.

[45] B. Mondal, A. Rana, P. Sen, A. Dey, *J. Am. Chem. Soc.* **2015**, *137*, 11214–11217.

[46] D. Mendoza, S. T. Dong, N. Kostopoulos, V. Pinty, O. Rivada-Wheelaghan, E. Anxolabéhère-Mallart, M. Robert, B. Lassalle-Kaiser, *ChemCatChem* **2023**, *15*, e202201298.

[47] D. P. Rillema, G. Allen, T. J. Meyen, D. Conrad, *Inorg. Chem.* **1983**, *22*, 1617–1622.

[48] B. Das, A. Rahaman, A. Shatskiy, O. Verho, M. D. Kärkäs, B. Åkermark, *Acc. Chem. Res.* **2021**, *54*, 3326–3337.

Entry for the Table of Contents

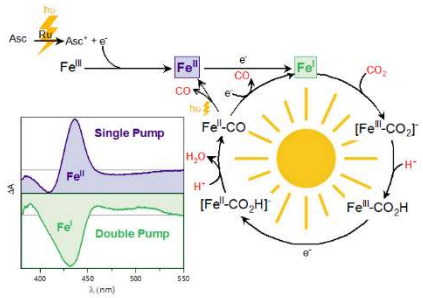

A pump-pump excitation strategy induces effective accumulation of charge on an Fe^{III}-based urea-modified porphyrin as the fates of the photogenerated species are tracked through their optical transient absorption signatures. In the presence of CO_2 as a substrate and H_2O as a proton source, the two-electron accumulated species leads to CO_2 activation and reduction, generating Fe^{II}-CO as a stable intermediate in the reaction mechanism.

Institute and/or researcher Twitter usernames: @ISMOlab_Orsay and @ICMMO-UMR8182